Noname manuscript No.
(will be inserted by the editor)

A 3D Collision Avoidance Strategy for UAVs in a Non-cooperative Environment

Xilin Yang · Luis Mejias Alvarez · Troy Bruggemann

Received: date / Accepted: date

Abstract This paper presents a feasible 3D collision avoidance approach for fixed-wing unmanned aerial vehicles (UAVs). The proposed strategy aims to achieve the desired relative bearing in the horizontal plane and relative elevation in the vertical plane so that the host aircraft is able to avoid collision with the intruder aircraft in 3D. The host aircraft will follow a desired trajectory in the collision avoidance course and resume the pre-arranged trajectory after collision is avoided. The approaching stopping condition is determined for the host aircraft to trigger an evasion maneuver to avoid collision in terms of measured heading. A switching controller is designed to achieve the spatial collision avoidance strategy. Simulation results demonstrate that the proposed approach can effectively avoid spatial collision, making it suitable for integration into flight control systems of UAVs.

Keywords UAV · collision avoidance · switching control · PID control

1 Introduction

There has been an increasing number of UAV applications in the past few years due to their usefulness in a variety of situations following the success of several projects such as the *Global Hawk* [1], the *Predator* [2] and the *MQ-8B Firescout* [3]. UAVs have shown several advantages over manned aircraft such as low manufacturing and operational costs (depending on the UAV type), flexibility to accommodate different payloads and risk reduction of human lives (no pilot or crew), etc. These advantages have enabled UAVs as an indispensable platform for various flight missions ranging from intelligence, surveillance and reconnaissance to scientific investigations and battlefield loss assessment.

Xilin Yang, Luis Mejias Alvarez and Troy Bruggemann
are with the Australian Research Center for Aerospace Automation
and Queensland University of Technology, Brisbane, Australia.
E-mail: {xilin.yang, luis.mejias, t.bruggemann}@qut.edu.au

The risk of unexpected spatial aircraft collision increases when they share the same airspace with other vehicles. This is caused by the fact that pre-arranged flight trajectories for UAVs are designed with little consideration of potential encounter. Also, the problem of UAV sense-and-avoid has been identified as one of the most significant challenges facing the integration of UAVs in the national airspace [4,5].

The collision avoidance problem can be divided in two parts. The "sensing or detection" and the "avoidance" aspects, respectively. In this paper, we address the avoidance aspect of the problem by proposing an approach for 3D collision avoidance in a non-cooperative scenario. Here, "non-cooperative environment "refers to an environment where a host aircraft has no prior information on the flight trajectory of an intruder and cooperative communication between them is unavailable. Non-cooperative approaches are the most challenging aspects of the problem given the high uncertainty in the intruder state. We have previously investigated the problem from the passive sensor perspective [6–9].

Planar (2D) aircraft avoidance has been subject to extensive investigation in a considerable number of papers, and significant efforts have been made to deal with different problems in various scenarios [10–13]. Kochenderfer *et al.* [14] presented a decision-theoretic approach to developing a collision avoidance logic using probabilistic models of aircraft behavior. The proposed methodology is aimed at meeting the safety level with guarantee while lowering the false alert rate and simplifying the process of re-optimizing the logic in response to variations in airspeed and sensor capabilities. Saunders *et al.* [15] assumed a vision processing unit that provides object segmentation and a range estimate to nearby obstacles. The proposed nonlinear guidance law attempts to maneuver the UAV in such a way that the obstacle is moved to the edge of the camera field of view (FOV), maintaining the obstacle on the edge of FOV guarantees that trajectory of the UAV is not on the collision course with the obstacle. There are also some approaches which rely greatly on availability of a high-integrity GPS and a continuous data-link (e.g. automatic dependent surveillance broadcast (ADSB) [16,17]).

Passive sensors also provide a means of identifying obstacles in different avoidance strategies [18–20]. Beyeler *et al.* [21] presented a novel control strategy for autonomous flight in the vicinity of obstacles with proximity of obstacles estimated using optic flow sensors. The proposed solution allows a UAV to fly and avoid obstacles using a simple sensor-to-actuator mapping by exploiting properties of translation-induced optic flow and the dynamics of flying platforms, thus eliminating the need for state information provided by GPS. Griffiths *et al.* [22] proposed an obstacle avoidance strategy based on the mapping information which utilizes laser range finder and optic flow sensors to detect the terrain. Flight tests were conducted to verify the feasibility of this method in real scenarios. A new passive approach to collision detection and avoidance with moving obstacles is proposed by Angelov *et al.*[23]. In this strategy, a maneuver based on the worst case scenario will be initiated

once a potential collision is detected. Afterwards, an optimal return to the pre-planned route will be executed.

The present research is part of efforts devoted to design a Sense and Avoid (SA) system for airspace collision avoidance. This system only relies on the detection of signals emanating from the targets themselves. Recently, motion detection using multiple cameras provides an attractive means of developing a SA system due to relatively low cost, size and power requirements for sensors. The basic paradigm of this technology is to use multiple cameras placed at different angles to create multiple views that, when combined, can allow for calculation of object vectors [24]. The challenge of motion detection is that a moving UAV makes it difficult to design a generic algorithm for different scenarios. Thus, various algorithms have been developed to deal with different scenarios to make distinction between the movement of the host aircraft and that of the intruder [25,24,26]. In practice, these algorithms cancel the movement of the UAV, including movement based on vehicle trajectory, as well for vibration from the UAV. Currently, there are only a few authors addressing spatial (3D) collision avoidance. Christodoulou *et al.* [27] formulated the confliction avoidance problem in three-dimension as a mixed-integer nonlinear programming problem, and the total flight time to avoid possible conflicts were obtained. In the present work, we aim to develop a 3D aircraft collision avoidance system based on measured heading information. During normal flight course, UAVs are commanded to achieve steady-state flight conditions for most of the flight duration. Therefore, it is reasonable to assume that both host aircraft and intruder are with constant velocity before the collision is detected. The relative bearing is also assumed to be measurable in the considered application. Cameras onboard the host aircraft are used to estimate the desired relative bearing and relative elevation with respect to the intruder aircraft during the approach process. The host aircraft resumes the pre-arranged route after collision avoidance. By completing these tasks, the intruder aircraft can be kept within the FOV of the camera. Moreover, a switching control system is designed to command the UAV to achieve collision avoidance during the encounter course.

The remainder of the paper is organized as follows: Section 2 describes collision avoidance in a 2D scenario. This is achieved by designing a planar spiral trajectory for the host aircraft. In Section 3, we extend the collision strategy to a 3D scenario where the host aircraft keeps the desired relative bearing with respect to the intruder aircraft and a relative elevation in the vertical direction. Design of the control system to implement the proposed collision strategy is given in Section 4. In Section 5, simulation results are given for typical 3D collision avoidance scenarios. Section 6 concludes this paper.

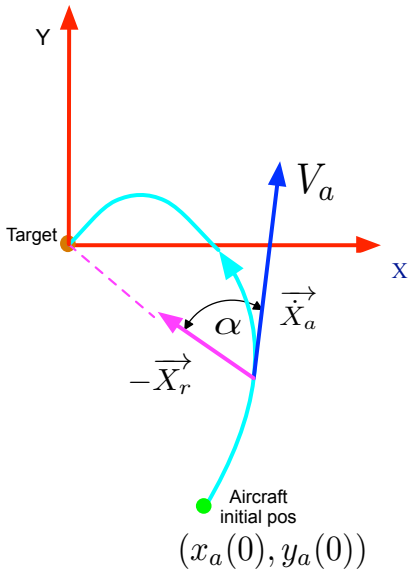

Fig. 1 A UAV approaches a stationary target keeping a constant bearing α

2 Collision Avoidance of a Stationary Target

In this section, we begin analyzing the trajectory followed when an aircraft maneuvers to avoid a stationary target. The collision avoidance problem is investigated in the planar case. Let us define, a polar and a Cartesian coordinate frames with both origins located at the position of the stationary target, as shown in Fig. 1. The aircraft starts from initial position $(x_a(0), y_a(0))$ with a constant speed of V_a. Any point on the maneuvering trajectory is described by (x_a, y_a) in Cartesian coordinates and (r, θ) in polar coordinates. Here, aircraft heading is denoted by θ which is the angle between $x-$axis and flight direction.

Theorem 1 *The path of an aircraft flying at a constant velocity V_a with a constant relative bearing α to a stationary target constructs an equiangular spiral trajectory.*

Proof: This proof is excerpted from [28]. Cartesian coordinate of the aircraft can be related to its polar coordinates by the following expression,

$$x_a(t) = r(t)\cos\theta(t) \tag{1}$$
$$y_a(t) = r(t)\sin\theta(t). \tag{2}$$

Differentiating these equations leads to

$$\dot{x}_a = \dot{r}\cos\theta - r\dot{\theta}\sin\theta \tag{3}$$
$$\dot{y}_a = \dot{r}\sin\theta + r\dot{\theta}\cos\theta. \tag{4}$$

It is observed from Fig. 1 that the relative bearing is the angle between flight direction $\dot{\mathbf{X}}_a$ and line-of-sight $(-\mathbf{X}_r)$. Here, relative range $\mathbf{X}_r$ is described by the vector (x_a, y_a). The constant bearing α indicates

$$\frac{\dot{\mathbf{X}}_a \cdot (-\mathbf{X}_r)}{\|\dot{\mathbf{X}}_a\|\|(-\mathbf{X}_r)\|} = \cos\alpha, \tag{5}$$

which takes the explicit form of

$$\frac{-(x_a\dot{x}_a + y_a\dot{y}_a)}{\sqrt{x_a^2 + y_a^2}\sqrt{\dot{x}_a^2 + \dot{y}_a^2}} = \frac{-\dot{r}}{\sqrt{\dot{r}^2 + \dot{\theta}^2 r^2}} = \cos\alpha. \tag{6}$$

The assumption that the aircraft approaches with a constant velocity V_a gives

$$\sqrt{\dot{x}_a^2 + \dot{y}_a^2} = \sqrt{\dot{r}^2 + \dot{\theta}^2 r^2} = V_a. \tag{7}$$

Thus, Eq. (6) can be rearranged as

$$\dot{r} = -V_a \cos\alpha, \tag{8}$$

and the solution can be obtained with initial condition $r(0) = r_0$

$$r(t) = -V_a t \cos\alpha + r_0. \tag{9}$$

Substituting Eq. (8) into Eq. (7) leads to a differential equation in terms of heading θ which yields the solution described by

$$\theta(t) = \theta_0 - \ln(1 - \frac{V_a t}{r_0}\cos\alpha)\tan\alpha, \tag{10}$$

subject to the time constraint $0 < t < r_0/(V_a \cos\alpha)$.

The trajectory can also be expressed in terms of range and heading by replacing time t in Eq. (9) with Eq. (10),

$$r(\theta) = r_0 e^{(\theta_0 - \theta)\cot\alpha}. \tag{11}$$

This is the equation of equiangular motion. For any point on the trajectory, the intersection angle between the flight direction and line-of-sight is constant α.

The following theorem gives the last time moment when the host aircraft should trigger an evasive maneuver. The time moment is only dependant on measurements of heading.

Theorem 2 *Given minimum range r_{min} (r_{min} is the radius of the minimum allowable flight circle), the aircraft can keep a constant relative bearing α during the encounter course until the time moment t^* given by*

$$t^* = \frac{r_0(1 - e^{(\theta_0 - \theta^*)\cot\alpha})}{V_a \cos\alpha}. \tag{12}$$

where the maximum allowable θ^* is determined by

$$\theta^* = -\tan\ln\frac{r_{min}}{r_0} + \theta_0, \tag{13}$$

and

$$\theta^* > \theta_0 \quad when \quad \alpha \in (0, \pi/2). \tag{14}$$

Proof: Given the minimum relative range r_{min}, the maximum allowable heading θ^* can be obtained from Eq. (11), which takes the form of Eq. (13). Therefore, the last time moment to trigger evasion maneuver for collision avoidance can be obtained from Eq. (10), which is expressed as Eq. (12).

It is noticed from Eq. (12) that the evasion time t^* is related to the initial relative range r_0. In our case, the only available information is heading angle θ and relative bearing α, and we proceed to estimate r_0 based on these information. We firstly collect sufficient measurements of $\theta_i, i = 1, ..., N$ where N indicates the number of samples. According to Eq. (11), relative range r_i at different sampling time is described by

$$r_i(\theta_i) = r_0 e^{(\theta_0 - \theta_i)\cot\alpha}, \ i = 1, ..., N, \tag{15}$$

which can be transformed into

$$\ln r_i = \ln r_0 + (\theta_0 - \theta_i)\cot\alpha, \ i = 1, ..., N \tag{16}$$

Introducing the following notation

$$x_i = \ln r_i, \ i = 0, \ldots, N \tag{17}$$

$$b_j = (\theta_0 - \theta_i)\cot\alpha, \ j = 1, \ldots, N, \tag{18}$$

converts Eq. (16) into a linear algebraic equation

$$AX = B, \tag{19}$$

where

$$A = \begin{bmatrix} -1 & 1 & & & \\ -1 & 0 & 1 & & \\ -1 & 0 & 0 & -1 & \\ \vdots & \vdots & \vdots & \vdots & \ddots \\ -1 & 0 & \cdots & \cdots & \cdots & 1 \end{bmatrix} \in R^{N\times(N+1)}; \tag{20}$$

$$X = [x_0, x_1, \cdots, x_N]^T \in R^{(N+1)\times 1}; \tag{21}$$

$$B = [b_1, \cdots, b_N]^T \in R^{N\times 1}. \tag{22}$$

Since the number of unknowns is larger than that of equations, equation (19) is under-determined and the minimum norm solution can be obtained which satisfies $min\|AX - B\|_2$. The solution takes the form of

$$\hat{X} = A^* B, \ A^* = A^T(AA^T)^{-1}, \tag{23}$$

where A^* is pseudo-inverse of A. Once the solution $\hat{X}$ is obtained, the initial relative range r_0 can be obtained using the Eq. (17). Measurement noise is an inevitable factor affecting estimation performance of the algorithm in real applications. In the considered application, white noise is added to measurements of heading to check performance of the proposed algorithm, shown in Section 5.

3 Spatial Collision Avoidance of a Moving Intruder

We consider avoiding the spatial collision with a moving intruder under constant speed assumptions during the encounter course. The relative bearing α_r and elevation β_r during the encounter course are described by

$$\alpha_r = \arctan \frac{y_a - y_t}{x_a - x_t}, \tag{24}$$

$$\beta_r = \arctan \frac{z_a - z_t}{x_a - x_t}, \tag{25}$$

where (x_a, y_a, z_a) are position coordinates of the host aircraft, and (x_t, y_t, z_t) are position coordinates of the intruder. The spatial encounter scenario assumes that the host aircraft and the intruder move with constant speeds towards each other and a potential collision will occur unless an avoidance maneuver is triggered. Here, the assumption that the intruder follows a straight flight with a constant velocity is reasonable since the encounter course does not persist for a long time and the intruder does not perform abrupt or aggressive maneuvers. When the host aircraft detects the intruder with the heading θ_0, relative range r_0 can be estimated using the method proposed in Section 2 based on measured heading collected up to the period of time when the encounter course occurs. Given the minimum allowable relative range, a switching controller is triggered to avoid the possible collisions and the aircraft is expected to maintain relative bearing α_r in the horizontal plane and relative elevation β_r in the vertical plane. This is implemented by design of controllers in consideration of actuator capability. After collision avoidance is achieved, the host aircraft is commanded by the switching controller to resume the prearranged flight trajectory. For a stationary object, the requirement that the relative bearing is constant generates a spiral horizontal approaching trajectory. For a moving intruder, it will be seen that, owing to the movement of relative kinematics, the resultant horizontal trajectory tends to be spiral-like during the collision avoidance course due to the variations in the relative bearing.

The kinematic equations used to describe motion of the aircraft are

$$\dot{x}_a = V_a \cos\theta \cos\gamma, \tag{26}$$

$$\dot{y}_a = V_a \sin\theta \cos\gamma, \tag{27}$$

$$\dot{z}_a = V_a \sin\gamma. \tag{28}$$

where $(\dot{x}_a, \dot{y}_a, \dot{z}_a)$ are velocity components of the aircraft. θ is heading angle and γ denotes flight path angle. The dynamic motion of velocity V_a, heading θ and flight path angles γ can be described by [29]

$$\dot{V}_a = \frac{1}{m}[Y \sin\beta + (T\cos a - D)\cos\beta] - g\sin\gamma, \tag{29}$$

$$\dot{\theta} = \frac{1}{mV_a\cos\gamma}[(L + T\sin a)\sin\sigma + Y\cos\sigma\cos\beta + (D - T\cos a)\cos\sigma\sin\beta], \tag{30}$$

$$\dot{\gamma} = \frac{1}{mV_a}[(L + T\sin a)\cos\sigma + (T\cos a - D) \cdot \sin\sigma\sin\beta - Y\sin\sigma\cos\beta] - \frac{1}{V_a}g\cos\gamma, \tag{31}$$

where V_a is the aircraft velocity, m the mass of the aircraft, g the gravitational acceleration, a the angle of attack, β the sideslip angle, γ the flight-path angle, σ the bank angle (rotation about the velocity vector), L the lift force, D the drag force and T the thrust force.

The lift force L is described as

$$\begin{aligned} L &= \bar{q}S_w C_L \\ C_L &= C_{L0} + C_L^a a + C_L^{\delta_f}\delta_f + C_L^{\delta_e}\delta_e \\ &\quad + \frac{c}{2V_a}(C_L^{\dot{a}}\dot{a} + C_L^q q) + C_L^M M. \end{aligned} \tag{32}$$

Here the dynamic pressure is $\bar{q} = 0.5\rho V_a^2$ and ρ is the air density. S_w is the wing planform area. Explanations to aerodynamic coefficients C_{L0} and $C_L^{(\cdot)}$ are given in [30]. δ_f and δ_e are flap and elevator control command. q and M are pitching rate and pitching moment.

Thrust T is given by

$$T = \bar{q}S_D T_c \tag{33}$$

where S_D is the area of disc swept out by a propeller blade and T_c is the thrust coefficient.

The drag force D is expressed as

$$\begin{aligned} D &= \bar{q}S_w C_D \\ C_D &= C_{D0} + \frac{(C_L - C_{L0})^2}{\pi e AR} + C_D^{\delta_f}\delta_f + C_D^{\delta_a}\delta_a \\ &\quad + C_D^{\delta_r}\delta_r + C_D^M M, \end{aligned} \tag{34}$$

and side force Y is

$$\begin{aligned} Y &= \bar{q}S_w C_Y \\ C_Y &= C_Y^\beta\beta + C_Y^{\delta_a}\delta_a + C_Y^{\delta_r}\delta_r + \frac{b}{2V_T}(C_Y^p p + C_Y^r r), \end{aligned} \tag{35}$$

Here, e is the efficiency factor and AR is the aspect ratio. δ_a and δ_r are aileron and rudder control command. Details for aerodynamic coefficients $T_c, C_D^{(\cdot)}$ and $C_Y^{(\cdot)}$ can be found in [30].

To construct a realistic collision scenario, the host aircraft is commanded to move with steady-state flight conditions. This indicates the velocity, angle of attack and pitch angle are kept constant, and accelerations and angular rates are stabilized to zero. For the UAV model, throttle, elevator and aileron are properly actuated to achieve steady-state flight in consideration of structural limitations and servo dynamics constraints. The thrust force is controlled by choosing appropriate angular speed of engine. Due to the absence of flaps and rudders onboard the UAV, bank and yaw motion are controlled through commanding aileron actuators. The bank-to-turn (BTT) control mechanism is employed and two proportional-integral-derivative (PID) controllers are designed. The first one takes the desired yaw motion as input and stabilizes the yaw motion to the desired level. The yaw error is then input into the BTT PID controller and the command is converted to actuate the aileron to stabilize the bank motion in consideration of roll limit. The pitch and altitude are controlled by deflecting the elevator and a PID controller is designed for this purpose.

The symmetric flight conditions $\beta = 0, Y = 0$ convert Eq. (29)-(31) into

$$\dot{V}_a = \frac{1}{m}((T\cos a - D) - g\sin\gamma), \tag{36}$$

$$\dot{\psi} = \frac{1}{mV_a\cos\gamma}(L + T\sin a)\sin\phi, \tag{37}$$

$$\dot{\gamma} = \frac{1}{mV_a}(L + T\sin a)\cos\phi - \frac{g\cos\gamma}{V_a}. \tag{38}$$

Here, we assume roll angle (ϕ) and bank angle (σ) are approximately equal due to the small quantity of the angle of attack a. When steady-state flight is achieved, the host aircraft moves with an constant velocity and yawing angle. Also, the stabilized pitch Θ and angle of attack a indicate that flight-path angle $\gamma = \Theta - a$ is also constant.

4 Design of the Switching Control System for Collision Avoidance

The control objective is to keep desired relative bearing α and relative elevation β during the encounter course. To implement the proposed strategy, a switching control scheme consisting of a pre-arranged controller and a collision avoidance controller is designed, as shown in Fig. 2. For free flight conditions, the pre-arranged controller generates flight trajectories in consideration of operational and flight envelope requirements. Normally, routine control algorithms are programmed and saved on the flight computer and the most suitable one is chosen for the specific airspace environment. Such a controller aims to achieve steady-state flight without consideration of the potential conflict collision. During the encounter course, the collision avoidance controller

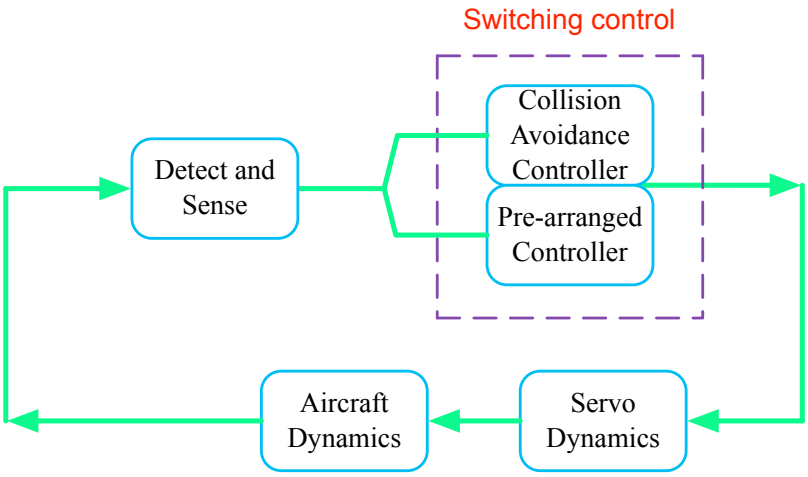

Fig. 2 The switching control system for collision avoidance

is triggered once the potential collision is identified by the detect and sense system on the host aircraft. It arranges an evasive flight trajectory subject to the constraints that the relative bearing and elevation are desired values.

It is found that the desired bearing of the host aircraft should be tuned to generate an anticipative flight trajectory subject to operational constraints when the aircraft is at close vicinity of the intruder. Practically, it is infeasible for the aircraft to consistently follow the spiral trajectory after collision avoidance is completed. Thus, as the aircraft is out of the potential collision region, pre-arranged flight control can be resumed.

A switching controller is introduced to initiate the collision avoidance controller when potential collision is detected, which is triggered by the estimated relative range (relative range is estimated in the horizontal plane). Once the relative range reaches the threshold, collision avoidance controller is activated to generate aileron and elevator command, i.e.,

$$\psi_{cmd} = \begin{cases} k_p^{\psi} e_1 + k_i^{\psi} \int e_1 dt + k_d^{\psi} \frac{de_1}{dt} & t < t_1 \\ k_p^{\psi} e_2 + k_i^{\psi} \int e_2 dt + k_d^{\psi} \frac{de_2}{dt} & t_1 < t < t_2 \\ 0, & t > t_2 \end{cases}$$

where $e_1 = \psi^d - \psi, e_2 = \arctan \frac{y_a - y_t}{x_a - x_t} + \alpha_r^d - \psi$. The term $\arctan \frac{y_a - y_t}{x_a - x_t} + \alpha_r^d$ denotes the desired yaw of the host aircraft during the encounter course. The yaw command ψ_{cmd} is subject to constraints $\psi_{min} \leq \psi_{cmd} \leq \psi_{max}$, and it resumes to zero after the collision avoidance is completed. (x_a, y_a) are horizontal positions of the host aircraft, and (x_t, y_t) of the intruder. k_p^{ψ}, k_i^{ψ} and k_d^{ψ} are proportional, integral and derivative gains of the PID controller. Zero yaw command indicates that current heading is the desired heading, and there is no need to drive the BTT to change the yawing. The host aircraft maintains the

current heading and travels in straight line. The time moment t_1 triggers the collision avoidance controller which is determined by the threshold of the estimated relative range. t_2 is the time moment to resume the straight-line flight after collision avoidance which is determined by the relative bearing angle α_r. This is the time when the relative bearing angle is less than a prescribed angle. The prescribed angle is defined by the relative angle between the two aircraft at time $t1$.

The collision avoidance also includes altitude control through deflecting the elevator. Initially, both the host aircraft and intruder move at the same altitude. Once the potential collision is detected, elevator of the host aircraft increases or decreases so that the host aircraft can ascend or descend to avoid the collision. When the collision is avoided, the host aircraft resumes level flight. In this case, the elevation can be considered as pitch, and the control command is

$$\Theta_{cmd} = k_p^{\Theta} e_3 + k_i^{\Theta} \int e_3 dt + k_d^{\Theta} \frac{de_3}{dt} \tag{39}$$

$$e_3 = \begin{cases} h^d - h & t < t_1 \\ h^d + \underbrace{h_c \tan(\arctan \frac{z_a - z_t}{x_a - x_t} + \beta_r^d - \Theta)}_{\text{Altitude correction term}} & t \geq t_1. \end{cases} \tag{40}$$

Here h^d is the desired altitude, h_c is a constant used to generate the desired altitude offset and $\arctan \frac{z_a - z_t}{x_a - x_t} + \beta_r^d$ is the desired elevation during the encounter course. $k_p^{\Theta}, k_i^{\Theta}$ and k_d^{Θ} are proportional, integral and derivative gains of the altitude PID controller. The altitude correction term aims to change altitude of the host aircraft to the desired level during the collision avoidance course.

5 Simulation Results

5.1 Performance of the Relative Range Estimation

In this section, we aim to evaluate the performance of the proposed relative range estimation method based on the measured heading angles θ when measurement noise is present. Here, the initial heading is $\theta_0 = 0$, and heading of the aircraft increases at an angular speed of $10\,\mathrm{deg}/s$. Equation (15) is employed to generate the heading information. A zero-mean Gaussian random noise is added to the heading measurements with normal distribution of $N(0, 0.02)$. The initial relative range r_0 is set to be 600 m. It is shown in simulations that range estimation accuracy is affected by the number of samples. Estimation accuracy degrades when an excessive large or a small number of samples are chosen. The proper number of samples is obtained when mean square errors between the real and estimated relative range reaches minimum. In the considered application as shown in Fig. 3, the number of samples is chosen to be 127.

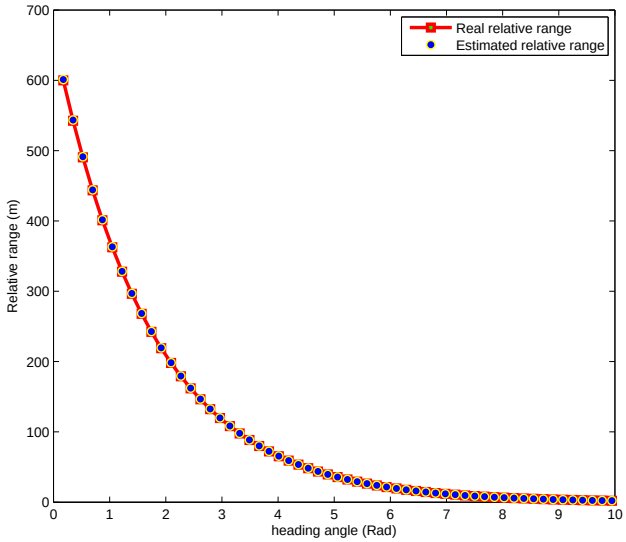

Fig. 3 Estimation of relative range using the proposed method

The sampled heading with measurement noise is used to construct the matrix A and vector B following Eq. (23). Once the solution $\hat{X}$ is obtained, the estimated relative range $r_i, i = 1, \ldots, N$ can be calculated from Eq. (17) (shown in Fig. 3). The estimated initial relative range $\hat{r}_0$ is 601.24 m, and the standard deviation for the estimated relative range is 0.38 m. It is observed that the proposed method can estimate the initial relative range with good accuracy.

5.2 Collision Avoidance for Typical Collision Scenarios

In this section, we tested performance of the control system for two typical collision scenarios when an intruder follows straight flight: head-on and angle interception. Also, the proposed strategy is applied to an intruder with a curved flight trajectory. Actuator constraints for aileron and elevator are also taken into account. It should be clarified that the proposed collision avoidance strategy can be applied to both manned and unmanned aircraft. Motivated by the availability of the Airborne Systems Laboratory (ASL) [31] as a flight ready testing capability with a reliable fault-tolerant flight control system[1], we decided to test the collision avoidance strategy using a Cessna model to validate, identify and remedy possible deficiencies before its implementation on UAVs

[1] It is worth noting that the ASL has autonomous capabilities. Collision avoidance algorithms running on an onboard payload can autonomously command the aircraft. Therefore much of its behavior is similar to a UAV.

with safety guarantees. For this purpose we use a high-fidelity Cessna aircraft model from the Airlib [32] simulation toolbox. The Airlib toolbox provides a graphical software environment in consideration of aeronautical constraints for the design and analysis of aircraft dynamics and control systems. Thus, employment of the Cessna 172 model from the Airlib leads to a reliable performance evaluation of the proposed strategy. Aerodynamic parameters of the Cessna, as shown in Table 1, are used in simulations to test performance of the proposed strategy.

For the head-on case, the host aircraft initially follows a level flight with 45^o heading. The intruder follows a straight line and moves towards the host aircraft. Both at an altitude of 60 m. Once the potential collision is detected based on the minimum allowable range, the host aircraft starts the collision avoidance strategy by keeping the relative bearing of 40^o and relative elevation of 5^o during the encounter course. Control gains for heading are chosen to be $k_p^{\psi} = 1.5$, $k_i^{\psi} = 0$ and $k_d^{\psi} = 0.05$. Control gains for pitch are $k_p^{\Theta} = -0.01, k_i^{\Theta} = -0.0021$ and $k_d^{\Theta} = -0.01$. Another PID controller is used to implement the BTT control to generate aileron command with control gains $k_p = -0.05, k_i = -0.1$ and $k_d = 0$. It is noticed from Fig. 4 that the host aircraft flies sideways on the horizontal plane and increases height to avoid collision. Once collision avoidance is achieved, the host aircraft resumes its pre-arranged route. For the angle interception scenario, the intruder aircraft moves with initial heading of 135^o and the host aircraft of 45^o. It is seen from Fig. 5 that the collision avoidance has been achieved when the desired relative bearing is 60^o and relative elevation is -35^o during the encounter course. The control gains are chosen to be $k_p = 0.7$ and $k_i = 12$. In Fig. 6, the intruder initially moves towards the host aircraft with a constant heading. During the encounter course, the intruder changes heading to follow a curved flight trajectory with varying velocity from 54 m/s to 56 m/s. In this case, potential collision is avoided by keeping a relative bearing of 30^o and relative elevation of 5^o. Control gains are $k_p^{\psi} = 1.7, k_i^{\psi} = 0, k_d^{\psi} = 0.045$ for the heading, and $k_p^{\Theta} = -0.02, k_i^{\Theta} = -0.004$, $k_d^{\Theta} = -0.015$ for the pitch. It is seen that the host aircraft follows a spiral trajectory in the horizontal plane and increases height to avoid the collision during the encounter course.

We investigate how the minimum relative range changes with variations in the desired relative bearing and elevation for the straight flight intruder. Table 2 summarizes the distribution of minimum relative range for different relative bearing and elevation. It is noticed that for a given relative elevation, the minimum relative range increases with an increase in relative bearing. This indicates that when the desired relative bearing is larger, the host aircraft tends to follow a spiral-like trajectory with a larger distance from the intruder. For a given desired relative bearing, the same trend can also be observed. Therefore, increasing relative bearing and elevation can help to avoid spatial collision with safety guarantees.

Table 1 Parameters of the Cessna 172

Parameters	Value
m: Gross mass with full tank	1043.3 kg
g: Gravitational acceleration	9.80665 ms^{-2}
ρ: Air density	1.201 kgm^{-3}
S: Aircraft wing area	16.17 m^2
b: Wing Span	10.91 m
I_{xx}: Moment of inertia about $x-$axis	1285.3 kgm^2
I_{yy}: Moment of inertia about $y-$axis	1824.9 kgm^2
I_{zz}: Moment of inertia about $z-$axis	2666.9 kgm^2
I_{xz}: Product of inertia	0
C_{L0}: Aircraft lift curve intercept	0.31
C_L^{α}: Aircraft lift curve slope	5.143
$C_L^{\dot{\alpha}}$: Change in lift coefficient with time rate of angle of attack	1.3714
$C_L^{\delta_e}$: Change in lift coefficient with elevator control	0.43
C_L^{q}: Change in lift coefficient with pitching	3.9
C_L^{M}: Change in lift coefficient with pitching moment	0
C_{D0}: Minimum drag	0.031
e: Efficiency factor	1
$\mathcal{AR}$: Aspect ratio	7.32
$C_D^{\delta_e}$: Elevator drag contribution	0.06
$C_D^{\delta_a}$: Aileron drag contribution	0.13
C_D^{M}: Change in drag coefficient with pitching moment	0
C_Y^{β}: change in side force coefficient with sideslip angle	-0.31
$C_Y^{\delta_a}$: Aileron effect on side fore coefficient	0
C_Y^{p}: Change in side force coefficient with rolling rate	-0.037
C_Y^{r}: Change in side force coefficient with yaw rate	0.21
C_l^{β}: Change in rolling moment coefficient with sideslip angle	-0.089
$C_l^{\delta_a}$: Change in rolling moment coefficient with aileron deflection	-0.178
C_l^{p}: Change in rolling moment coefficient with roll rate	-0.47
C_l^{r}: Change in rolling moment coefficient with yaw rate	0.096
C_{m0}: Zero lift pitching moment coefficient	-0.015
C_m^{α}: Change in pitching moment coefficient with angle of attack	-0.89
$C_m^{\delta_e}$: Change in pitching moment coefficient with elevator deflection	-1.28
$C_m^{\dot{\alpha}}$: Change in pitching moment coefficient with time rate of angle of attack	-4.8438
C_m^{q}: Change in pitching moment coefficient with pitching rate	-12.4
C_m^{M}: Change in pitching moment coefficient with pitching moment	0
C_n^{β}: Change in yaw moment coefficient with sideslip angle	0.065
$C_n^{\delta_a}$: Change in yaw moment coefficient with aileron deflection	-0.053
C_n^{p}: Change in yaw moment coefficient with rolling rate	-0.03
C_n^{r}: Change in yaw moment coefficient with yaw rate	-0.099

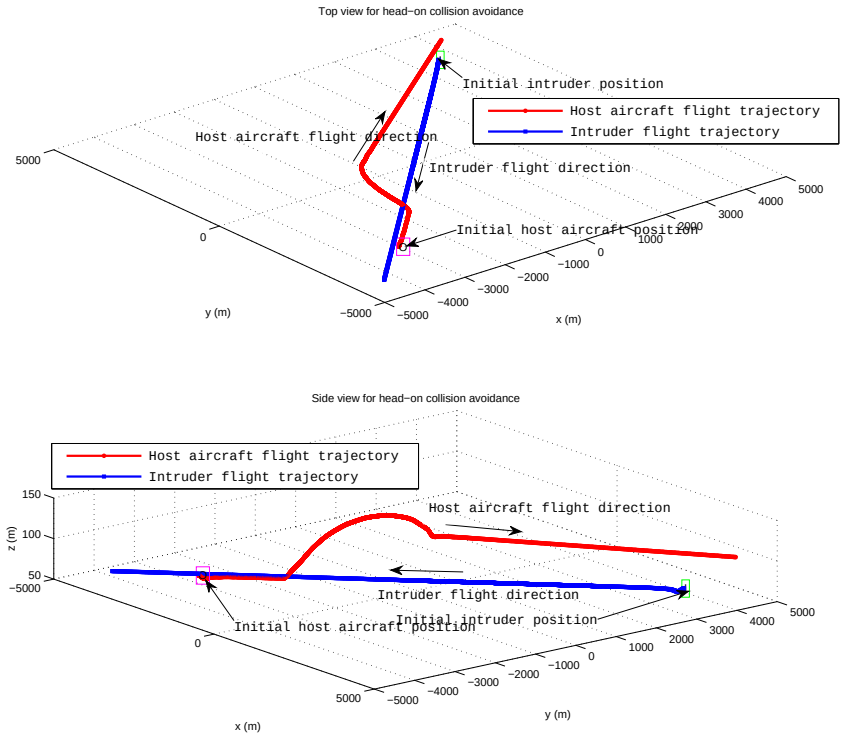

Fig. 4 Collision avoidance for the head-on scenario

6 Conclusion and future work

In this paper, a feasible spatial collision avoidance strategy is proposed. The host UAV is controlled to maintain a safe relative range from the intruder by keeping the desired relative bearing and elevation during the collision course. The switching control system is also designed to determine the time moment to trigger the collision avoidance strategy. Performance of the proposed collision avoidance strategy is verified in typical collision scenarios. It is demonstrated that the collision avoidance can be achieved using the proposed strategy. We are currently working towards the implementation of this approach on our ASL platform where the simulated scenarios presented here will be tested using two aircraft. Future work also includes testing the proposed strategy for scenarios when UAVs are with variable velocity.

Acknowledgements This research was supported under Australian Research Council's Linkage Projects funding scheme (project number LP100100302) and the Smart Skies Project, which is funded, in part, by the Queensland State Government Smart State Funding Scheme.

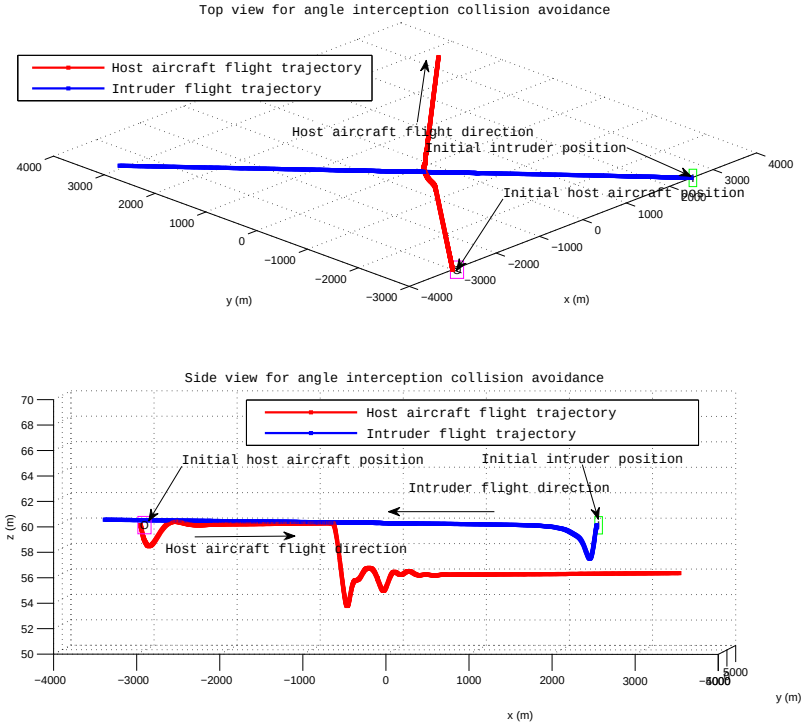

Fig. 5 Collision avoidance for angle interception scenario

References

1. N. J. S. Stacy, D. W. Craig, J. Staromlynska, and R. Smith, "The global hawk UAV australian deployment: Imaging radar sensor modifications and employment for maritime surveillance," in *IEEE International Geoscience and Remote Sensing Symposium*, vol. 2, 2002, pp. 699 – 701.
2. J. G. Drew, R. Shaver, K. F. Lynch, M. A. Amouzegar, and D. Snyder, *Unmanned aerial vehicle end-to-end support considerations*. RAND Corporation, 2005.
3. J. Downs, R. Prentice, S. Dalzell, A. Besachio, C. M. Ivler, M. B. Tischler, and M. H. Mansur, "Control system development and flight test experience with the MQ-8B fire scout vertical take-off unmanned aerial vehicle (VTUAV)," in *American Helicopter Society 63rd Annual Forum*. Virginia Beach, VA: May, 2007.
4. M. T. DeGarmo, "Issues concerning integration of unmanned aerial vehicles in civil airspace," MITRE, Tech. Rep., 2004.
5. O. of the Secretary of Defense, *Unmanned Systems Roadmap*. Department of Defense, 2007.
6. L. Mejias, J. Ford, and J. Lai, "Towards the implementation of vision-based UAS sense-and-avoid." in *Proceedings of the 27th International Congress of the Aeronautical Sciences (ICAS 2010 CD-Rom)*, 2010.
7. L. Mejias, S. Mcnamara, J. Lai, and J. J. Ford, "Vision-based detection and tracking of aerial targets for uav collision avoidance," in *Proceedings of the 2010 IEEE/RSJ International Conference on Intelligent Robots and Systems (IROS)*, October 2010, pp. 87–92.

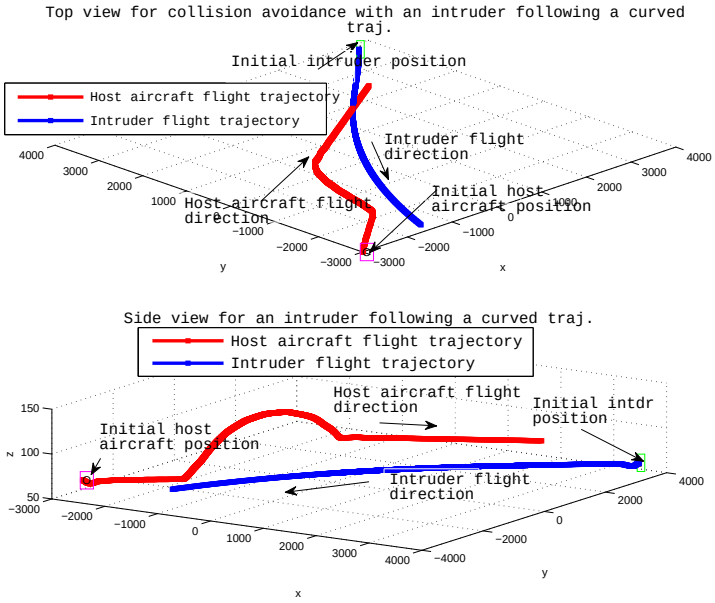

Fig. 6 Collision avoidance for the intruder with a curved flight trajectory

Table 2 Minimum Relative Range for Head-on Collision Avoidance for the Straight Flight Intruder

	Rel. bearing α_r				
Rel. elevation β_r	25^o	30^o	35^o	40^o	45^o
5^o	1191.07	1304.04	1428.60	1561.37	1698.01
6^o	1240.49	1349.71	1470.98	1600.49	1733.35
7^o	1290.93	1396.08	1514.18	1640.67	1769.69
8^o	1341.19	1443.12	1557.83	1681.75	1806.98
9^o	1404.91	1495.74	1602.40	1723.47	1845.20
10^o	1436.49	1568.98	1656.93	1765.29	1884.40
11^o	1493.47	1574.88	1733.81	1815.49	1924.63
12^o	1523.02	1671.25	1743.40	1883.16	1965.63
13^o	1613.41	1674.78	1779.70	1891.94	2017.95
14^o	1682.81	1750.93	1792.57	1918.30	2034.67
15^o	1725.52	1806.63	1843.64	2062.97	2160.20

8. J. Lai, L. Mejias, and J. J. Ford, "Airborne Vision-based Collision-Detection System," *Journal of Field Robotics*, vol. 28, no. 2, pp. 137–157, 2011.
9. J. S. Lai, J. J. Ford, L. Mejias, P. J. O'Shea, and R. A. Walker, "Detection versus false alarm characterisation of a vision-based airborne dim-target collision detection system," in *DICTA 2011 : Digital Image Computing : Techniques and Applications*, Noosa, QLD, December 2011. [Online]. Available: http://eprints.qut.edu.au/46624/
10. S. Han, H. Bang, and C. Yoo, "Proportional navigation-based collision avoidance for uavs," *International Journal of Control, Automation, and Systems*, vol. 7, no. 4, pp.

553–565, 2009.
11. N. F. T. Tarnopolskaya, "Optimal cooperative collision avoidance strategy for coplanar encounter: Merz's solution revisited," *Journal of Optimization Theory and Applications*, vol. 140, pp. 355–375, 2009.
12. G. Roussos and K. J. Kyriakopoulos, "Towards constant velocity navigation and collision avoidance for autonomous nonholonomic aircraft-like vehicles," in *Joint 48th IEEE Conference on Decision and Control and 28th Chinese Control Conference*, Shanghai, China, Dec. 2009, pp. 5661–5666.
13. D. H. Shim and S. Sastry, "An evasive maneuvering algorithm for uavs in see-and-avoid situations," in *Proceedings of the American Control Conference*, New York City, USA, Jul. 2007, pp. 3886–3892.
14. M. J. Kochenderfer, J. P. Chryssanthacopoulos, L. P. Kaelbling, and T. Lozano-Perez, "Model-based optimization of airborne collision avoidance logic," MIT, Lincoln Laboratory, Tech. Rep., 2010.
15. J. Saunders and R. Beard, "Reactive vision based obstacle avoidance with camera field of view constraints," in *AIAA Guidance, Navigation and Control Conference and Exhibit*, Honolulu, Hawaii, Aug. 2008.
16. S. Shandy and J. Valasek, "Intelligent agent for aircraft collision avoidance," in *AIAA Guidance, Navigation and Control Conference and Exhibit*, Montreal, Canada, Aug. 2001, pp. AIAA–2001–4055.
17. R. Holdsworth, "Autonomous in-flight plan planning to replace pure collision avoidance for free free aircraft using automatic dependent surveillance broadcast," Ph.D. dissertation, Department of Electrical Engineering at Swinburne University, Nov. 2003.
18. A. Viquerat, L. Blackhall, A. Reid, S. Sukkarieh, and G. Brooker, "Reactive collision avoidance for unmanned aerial vehicle using Doppler radar," in *6th International Conference on Field and Service Robotics-FSR 2007*, Dec. 2007.
19. H. Voos, "UAV "see and avoid" with nonlinear filtering and non-cooperative avoidance," in *Proc. 13th IASTED Int. Conf. Robotics and Applications*, Wurzburg, Germany, 2007.
20. O. Shakernia, W. Z. Chen, and V. M. Raska, "Passive ranging for uav sense and avoid applications," in *Proc. AIAA Infotech@Aerospace Conf.*, Arlington, Virginia, 2005, pp. 1–10.
21. A. Beyeler, J. C. Zufferey, and D. Floreano, "Vision-based control of near-obstacle flight," *Autonomous Robots*, vol. 27, no. 3, pp. 201–219, 2009.
22. S. Griffiths, J. Saunders, A. Curtis, B. Barber, T. McLain, and R. Beard, "Obstacle and terrain avoidance for miniature aerial vehicles," in *Advances in Unmanned Aerial Vehicles*. Springer, 2007, pp. 213–244.
23. P. Angelov, C. D. Bocaniala, C. Xideas, C. Patchett, D. Ansell, M. Everett, and G. Leng, "A passive approach to autonomous collision detection and avoidance in uninhabited aerial systems," in *Proc. 10th Int. Conf. on Computer Modeling and Sim.*, Cambridge, U.K., 2008, pp. 64–69.
24. M. Shah, A. Hakeem, and A. Basharat, "Detection and tracking of objects from multiple airborne cameras," *The International Society for Optical Engineering*, 2006.
25. D. J. Lee, R. W. Beard, P. C. Merrell, and P. Zhan, "See and avoidance behaviors for autonomous navigation," *SPIT optics east, robotics technologies and architechture, mobile robot XVII*, vol. 5609-05, 2004.
26. K. Nordberg, P. Doherty, G. Farneback, P. E.-F. G.Granlund, A. Moe, and J. Wiklund, "vision for a UAV helicopter," in *Proc. IROS'02 workshop on aerial robotics*, 2002.
27. M. A. Christodoulou and S. G. Kodaxakis, "Automatic commercial aircraft-collision avoidance in free flight: The three-dimensional problem," *IEEE transactions on intelligent transportation systems*, vol. 7, pp. 242–249, 2006.
28. K. N. Boyadzhiev, "Spirals and conchospirals in the flight of insects," *The College Mathematics Journal*, vol. 30, no. 1, pp. 23–31, 1999.
29. G. Ambrosino, M. Ariola, U. Ciniglio, F. Corraro, E. D. Lellis, and A. Pironti, "Path generation and tracking in 3-D for UAVs," *IEEE Transactions on Control Systems Technology*, vol. 17, no. 4, 2009.
30. B. L. Stevens and F. L. Lewis, *Aircraft Control and Simulation*, 2nd ed. John Wiley and Sons, Inc., 2003.

31. D. Greer, R. Mudford, D. Dusha, and R. Walker, "Airborne systems laboratory for automation research," in *27th International Congress of the Aeronautical Sciences*, 2010.
32. M. Rauw, *FDC 1.2-A SIMULINK Toolbox for Flight Dynamics and Control Analysis*, 2^{nd} ed. M. O. Rauw, May 2001.